Graphene with Covalently Grafted Amino Acid as a Route Toward Eco-Friendly and Sustainable Supercapacitors

Eleni C. Vermisoglou,[a] Petr Jakubec,[a] Aristides Bakandritsos,[a, b] Vojtěch Kupka,[a] Martin Pykal,[a] Veronika Šedajová,[a, c] Jakub Vlček,[c] Ondřej Tomanec,[a] Magdalena Scheibe,[a] Radek Zbořil,[a, b] and Michal Otyepka*[a, d]

Eco-friendly, electrochemically active electrode materials based on covalent graphene derivatives offer enormous potential for energy storage applications. However, covalent grafting of functional groups onto the graphene surface is challenging due to its low reactivity. Here, fluorographene chemistry was employed to graft an arginine moiety via its guanidine group homogeneously on both sides of graphene. By tuning the reaction conditions and adding a non-toxic pore-forming agent, an optimum degree of functionalization and hierarchical porosity was achieved in the material. This tripled the specific surface area and yielded a high capacitance value of approximately 390 $F g^{-1}$ at a current density of 0.25 $A g^{-1}$. The applicability of the electrode material was investigated under typical operating conditions by testing an assembled supercapacitor device for up to 30000 charging/discharging cycles, revealing capacitance retention of 82.3%. This work enables the preparation of graphene derivatives with covalently grafted amino acids for technologically important applications, such as supercapacitor-based energy storage.

Introduction

Depleted natural resources, such as fossil fuels, and severe environmental pollution problems related to the greenhouse effect and global warming as well as ever-growing energy consumption have prompted the search for clean energy sources and renewable energy storage technologies.[1] Electrochemical energy storage devices utilize physical-chemical processes to store electricity. Rechargeable batteries and supercapacitors have attracted great attention in applications concerning hybrid electric vehicles, mobile electronics, and smart displays.[2,3] Even though rechargeable batteries can store large amounts of energy (i.e., enable a high energy density) they provide a low power density due to long charge/discharge times. Moreover, they often suffer from poor lifecycle stability, which restricts their versatility. In contrast, supercapacitors achieve a high power density and long cycle lifetimes, and significant efforts to improve their relatively low energy density have been made worldwide.[4,5] Ultra-long electrochemical stability and slow aging are fundamental requirements for cutting-edge technology products.[6]

Graphene, an allotrope of carbon in the form of a monolayer, appears to be excellent candidate for supercapacitor electrode material due to its huge theoretical specific surface area (SSA, 2675 $m^2 g^{-1}$), high conductivity, and intrinsic mechanical strength, giving rise to a specific capacitance of 550 $F g^{-1}$.[7–9] This lightweight and flexible material may exhibit much lower values of specific capacitance due to irreversible restacking and agglomeration upon preparation processes as a result of graphene interlayer van der Waals forces. Consequently, the active surface area accessible to electrolyte ions is significantly reduced.[10] Functionalization of graphene with small biocompatible organic molecules that can act as spacer materials prevents the aggregation of graphene sheets, facilitating ion transfer. Furthermore, bio-organic functionalities are renewable, typically low cost, allow rational design synthesis, and generate minimum waste.[11] These low-molecular units afford extra redox sites, contributing pseudocapacitance to the overall capacitance. So far, only a few electrode materials have been prepared by functionalization of graphene with biocompatible organic molecules (Table S1 in the Supporting Information). In 2017, El-Gendy et al. reported the covalent functionalization of spongy graphene with biocompatible adenine, where the labile oxygen groups of graphite oxide (GO) were covalently

[a] Dr. E. C. Vermisoglou, Dr. P. Jakubec, Dr. A. Bakandritsos, Dr. V. Kupka, Dr. M. Pykal, V. Šedajová, O. Tomanec, Dr. M. Scheibe, Prof. Dr. R. Zbořil, Prof. Dr. M. Otyepka
Czech Advanced Technology and Research Institute (CATRIN)
Regional Centre of Advanced Technologies and Materials (RCPTM)
Palacký University Olomouc
Šlechtitelů 27, 779 00 Olomouc (Czech Republic)
E-mail: Michal.Otyepka@upol.cz
[b] Dr. A. Bakandritsos, Prof. Dr. R. Zbořil
Nanotechnology Centre,
Centre of Energy and Environmental Technologies
VŠB–Technical University of Ostrava
17. listopadu 2172/15, 708 00 Ostrava-Poruba (Czech Republic)
[c] V. Šedajová, Dr. J. Vlček
Department of Physical Chemistry,
Faculty of Science
Palacký University Olomouc
17. listopadu 12, 771 46 Olomouc (Czech Republic)
[d] Prof. Dr. M. Otyepka
IT4Innovations,
VSB–Technical University of Ostrava
17. listopadu 2172/15, 708 00 Ostrava-Poruba (Czech Republic)

Supporting information for this article is available on the WWW under https://doi.org/10.1002/cssc.202101039

bound to the amino groups of adenine, for preparing green and high-performance supercapacitors. A capacitance of 322.1 $F g^{-1}$ at a current density of 1 $A g^{-1}$ was achieved using aqueous 0.5 M H_2SO_4 as an electrolyte in a three-electrode system. The material was tested for 1000 charging/discharging cycles and exhibited capacitance retention of 102%.[12] However, tests in a two-electrode setup corresponding more closely to real capacitor devices have not yet been performed. In 2020, Deng et al. presented the non-covalent functionalization of graphene with methylene blue as a binder-free electrode for solid-state supercapacitors. The material had an outstanding capacitance of 517 $F g^{-1}$ at a current density of 0.5 $A g^{-1}$ using aqueous 0.5 M H_2SO_4 as an electrolyte in a three-electrode setup. The corresponding device showed capacitance retention of 72% in 10000 charging/discharging cycles in H_2SO_4/polyvinyl alcohol (PVA) electrolyte.[13] Zhou et al. confined methylene blue in three-dimensional reduced graphene oxide, and the prepared electrode material displayed a capacitance of 311 $F g^{-1}$ at a current density of 1 $A g^{-1}$ using 1 M H_2SO_4 as an electrolyte in a three-electrode setup. The capacitance retention for 10000 cycles was 96%. The material in a device exhibited capacitance retention of 81% for 10000 cycles using PVA/H_2SO_4 as an electrolyte.[14] However, non-covalently functionalized materials are susceptible to spontaneous disintegration. Therefore, it is desirable to prepare covalently functionalized graphene using biocompatible organic molecules. Covalent functionalization compared to non-covalent functionalization has the benefits of stability and controllability of the structure, enabling better processability.[15] The functionality is fixed on graphene and cannot easily be detached into the electrolyte solution. Therefore, the integrity of the material is preserved for a longer time.[16]

Direct covalent functionalization of graphene is hard to achieve. However, the use of fluorographene (FG) chemistry bypasses this obstacle, enabling a wide portfolio of graphene derivatives to be synthesized with grafted functional groups. The source of FG (i.e., graphite fluoride) is abundant since it is produced in tons industrially to be used as a lubricant. Further, FG has a well-defined structure, that is, a hexagonal lattice of sp^3 carbons homogeneously bonded to fluorine atoms. FG is easily susceptible to nucleophilic attack, reacting readily with amines, alcohols, thiols, and others.[17–19]

In the present work, the synthesis of zwitterionic arginine-functionalized FG (FG/Arg) is reported. Owing to the guanidino functional group, Arg can act as a nucleophile and can be grafted onto FG through nucleophilic attack, initiated on the electrophilic radical centers at the defect sites of FG.[20,21] To avoid random grafting of Arg on FG, the functionalization initially employed *tert*-butoxycarbonyl (Boc)-protected Arg, which was afterwards deprotected. Different reaction times were investigated to optimize the reaction conditions in terms of the defluorination (increasing the conductivity) and functionalization degree (FD, increasing the zwitterionic character benefiting the capacitance[22]). The derivative with the optimum porosity exhibited the maximum capacitive performance, which was further improved by adding potassium carbonate (K_2CO_3). The surface area was increased by a factor of around 3, and (in addition to the existing mesoporosity) micropores (centered at ≈1.5 nm) were developed in situ during the reaction, yielding a hierarchically porous derivative. The impact of hierarchical porosity was profound, increasing the capacitance by 30% in comparison to the derivative without K_2CO_3 treatment, reaching 390 $F g^{-1}$ at a current density of 0.25 $A g^{-1}$. These findings show that the present strategy can tune three key features of graphene derivatives (conductivity, FD, and porosity), significantly enhancing the capacitance of the products.[23] The synthesized material represents an eco-friendly Arg-functionalized graphene that could be used as an efficient supercapacitor in aqueous electrolytes. This work opens new avenues for grafting amino acids onto a graphene surface. Owing to the N- and C-termini, such graphenes could be useful in many applications, including biosensing, analytical chemistry, and others.

Results and Discussion

The strategy used for the specific covalent functionalization of FG with Arg is summarized in Figure 1a. First, the available primary guanidino amine of Boc-Arg-OH was reacted with FG through nucleophilic attack and then de-protection was carried out by treatment of FG/Boc-48 h with hydrochloric acid under heating. The successful removal of the Boc protecting group and presence of a free α-amino group in the produced FG/Arg-48 h were confirmed by the Kaiser test and Fourier-transform

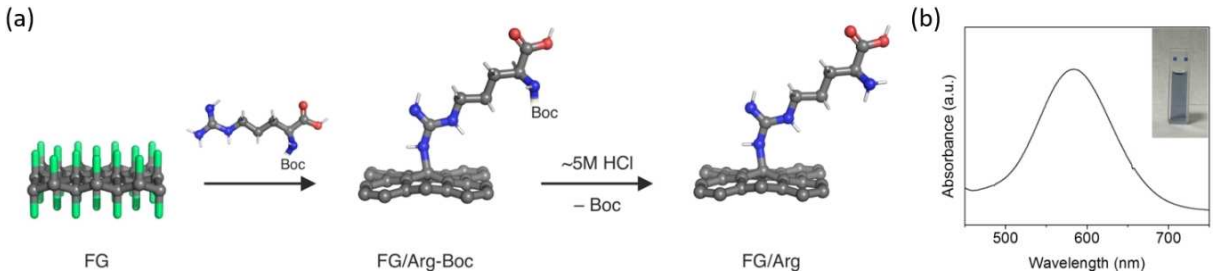

Figure 1. (a) Scheme illustrating FG reaction with Boc-Arg-OH and subsequent removal of the Boc protecting group to generate the FG/Arg product (hydrogens are not shown). Color of important elements in 3D visualization of molecules is coded as follows: carbon = grey; fluorine = green; nitrogen = blue; oxygen = red. (b) Kaiser test of FG/Arg-48 h sample.

(FT)IR measurements. Reaction with ninhydrin generated a deep blue solution (with absorption maximum at ≈583 nm, Figure 1b), whereas in the absence of FG/Arg-48 h, both FG/Boc-48 h and the blank solutions were colorless (Figure S1).

Direct evidence for the functionalization of GrF with Arg was obtained from FTIR measurements of GrF, FG/Boc-48 h, and FG/Arg-48 h samples. The FTIR spectrum of GrF (Figure 2a) showed a characteristic strong band at 1204 cm^{-1} and weaker band at 1307 cm^{-1} assigned to stretching vibrations of covalent C–F bonds and peripheral C–F_2 bonds, respectively.[23,24] The spectrum of FG/Boc-48 h showed the characteristic band of N–H stretching vibrations at around 3187 cm^{-1}, which was attributed to the secondary amine, and a band at around 3341 cm^{-1}, which was assigned to O–H stretching vibrations. In the case of FG/Arg-48 h, the O–H stretching vibration overlapped with a second N–H stretching vibration band attributed to the deprotected primary amine.[25,26] Two weak bands at around 2800–2950 cm^{-1} in the FG/Boc-48 h spectrum were attributed to C–H stretching vibrations of methyls present in the Boc protecting group.[25] A stretching vibration of the C=O group in the Boc protecting group was detected in the FG/Boc-48 h spectrum at around 1670 cm^{-1} but was absent in the FG/Arg-48 h spectrum, indicating effective de-protection of the Arg primary amine.[26] An absorption band at approximately 1571 cm^{-1} was suggested to be related to C=C skeleton vibrations in aromatic graphene regions in FG/Boc-48 h and also N–H bending vibration of the primary amine in FG/Arg-48 h.[24,26] A band at around 1400 cm^{-1} was assigned to either C–O–H bending due to a carboxylic group and/or C–N stretching vibration and –CH_2 deformation.[27–29] A band at approximately 1451 cm^{-1} was also attributed to –CH_2 bending vibration.[25] Broad strong bands centered at around 1207 cm^{-1} for FG/Boc-48 h and 1181 cm^{-1} for FG/Arg-48 h were assigned to C–F stretching vibration (≈1200 cm^{-1}) and C–N vibration (1000–1250 cm^{-1}).[30,31] The intensity ratio (>1.5) of the bands attributed to aromatic graphene and C–F stretching vibration in FG/Arg-48 h_K and FG/Arg-48 h indicated extensive graphitization and effective defluorination of the functionalized FG (Figure S2a). All the FTIR spectra are presented in Figure S2b.

Changes in the surface chemistry of graphene derivatives as a function of reaction time and upon addition of potassium carbonate to the reaction were elucidated by X-ray photoelectron spectroscopy (XPS). The results showed a significant loss of F atoms with time up to 48 h and greater elimination of F atoms for the sample prepared under alkaline conditions (FG/Arg-48_K) (Table 1).

High-resolution C 1 s XPS spectra of the parent material GrF and the covalently functionalized graphene derivative FG/Arg-48 h are presented in Figure 2b. The C 1 s peak was deconvoluted into six components in the case of GrF and 5 components

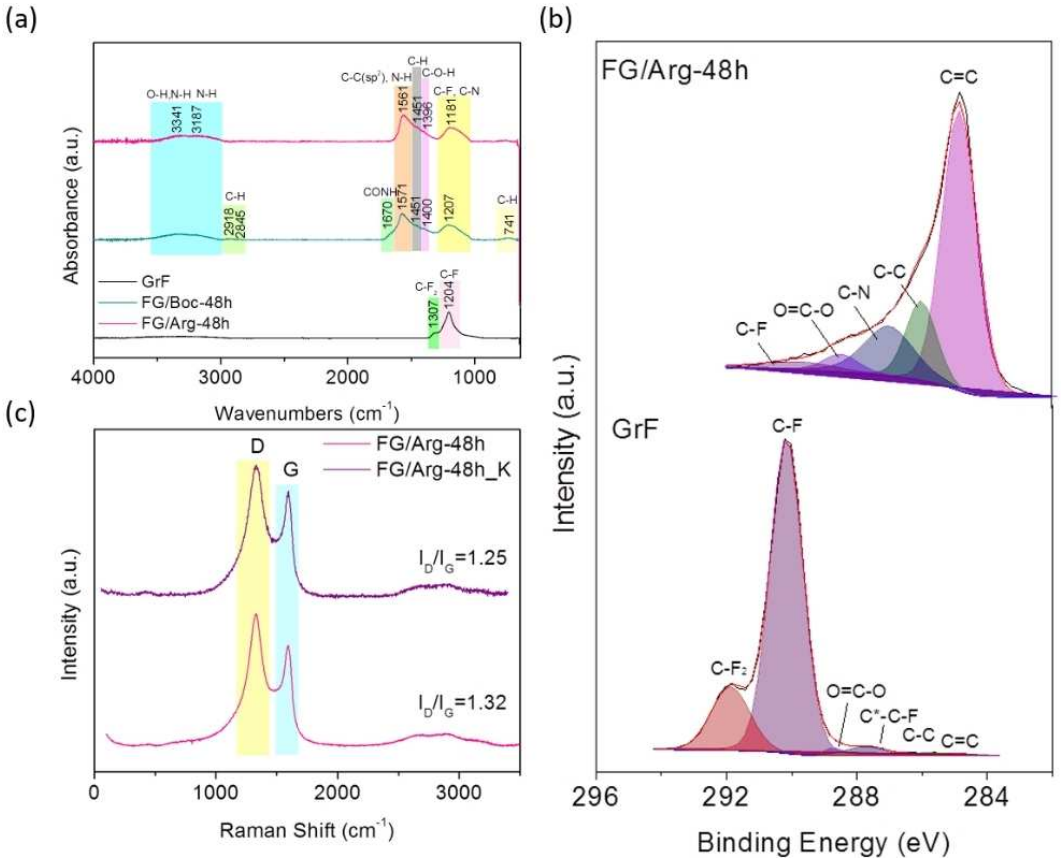

Figure 2. (a) FTIR spectra of GrF, FG/Boc-48 h, and FG/Arg-48 h. (b) High-resolution C 1 s XPS spectra of the parent material GrF and final product FG/Arg-48 h. (c) Raman spectra of FG/Arg-48 h and FG/Arg-48 h_K samples.

Table 1. Atomic composition of GrF, FG/Arg-xh (*x*: 24, 48, and 72 h)and FG/Arg-48 h_K samples derived from XPS analyses..

Sample	Element content [at%]				C/F
	C	N	O	F	
GrF	44.1	-	0.2	55.7	0.8
FG/Arg-24 h	78.4	10.6	6.0	5.0	15.7
FG/Arg-48 h	76.4	13.7	6.6	3.3	23.2
FG/Arg-72 h	77.2	13.2	6.3	3.3	23.4
FG/Arg-48_K	77.9	13.6	6.5	2.0	39.0

for the derivatives FG/Arg-xh (*x*: 24, 48, 72 h) and FG/Arg-48 h_K. The presence of a C–C (sp^2) bond was denoted by the peak located at around 284.81 eV, while the presence of C–C (sp^3), C–N, C*–C–F, O=C–O, C–F, and CF_2 bonds was implied by the peaks centered around 285.97, 287.17, 287.84, 288.61, 289.87, and 291.83 eV, respectively. XPS spectra of all the samples are shown in Figure S3. As the reaction time was increased, the atomic percentage of C–F decreased, reaching a value of 4.3 at 48 h, before remaining constant with further increases of time. This C–F content was lower for the sample prepared in the presence of potassium carbonate. The atomic percentage of C atoms bound in C=C (sp^2) was maximum at 24 h and then decreased with increasing time, whereas C atoms bound in C–C (sp^3) showed the inverse trend. Similar trends were observed for the sample prepared in the presence of potassium carbonate. Values for the content of C atoms participating in C–N and O=C–O groups indicative of FD were maximum for the sample prepared at 48 h (Table 2).

To estimate FD of the graphene derivatives, we combined results from thermogravimetric analysis (TGA) and XPS data. TGA of Arg as well as derivative thermogravimetry (DTG) graphs of all the samples are presented in Figure S4a,b. An example of the FD calculations is presented in the Supporting Information. For samples prepared at 24, 48, and 72 h, the corresponding FDs reached 2.9, 3.7, and 3.3, respectively. FD of FG/Arg-48 h_K was 3.5. The FD, low content of F atoms, and high content of sp^2 C atoms may indicate reasonable conductivity of the graphene with grafted Arg.

Raman spectra of the samples confirmed formation of the functionalized graphene derivative. Two prominent and rather wide D (1332 cm^{-1}) and G (1595 cm^{-1}) bands were present in the spectra. A high intensity ratio $I_D/I_G \approx 1.32$ (>1) for FG/Arg-48 h reflected the high FD due to the presence of sp^3 hybridized carbon atoms.[22,23] Nevertheless, carbon sp^2 hybridized atoms constituted a dominant fraction, giving rise to an intense G peak. It should be noted that the parent material GrF is a Raman-silent material.[32] The I_D/I_G ratio increased with increasing FD (Figures 2c and S5). The sample FG/Arg-48 h had the highest FD (3.7) as well as the highest I_D/I_G ratio (1.32). The slightly lower I_D/I_G ratio for the FG/Arg-48 h_K sample could reflect the role of the pore-forming agent, which may etch the less ordered carbon phase, increasing the sp^2 content in the sample.

When the covalently functionalized derivatives were dispersed in water, a zwitterionic network was formed, as shown by zeta potential ζp measurements as a function of pH (Figure 3a). The FG/Arg-48 h sheets in an aqueous environment were positively charged (up to +36.8 mV) due to protonation of the amino groups (pH 3.0–8.0). The isoelectric point (IEP) of FG/Arg-48 h was estimated to be around 8 (7.9), shifted from the isoelectric point of Arg (10.8) This pronounced shift of IEP can be considered indirect proof of Arg grafting via the

Table 2. Atomic percentage (at%) of characteristic groups in FG/Arg-xh derivatives and the parent GrF obtained from deconvolution of high-resolution C 1 s core level XPS spectra.

Sample	Group content [at%]						
	C–C (sp^2) ≈284.81 eV	C–C (sp^3) ≈285.97 eV	C–N ≈287.17	C*–C–F ≈287.84 eV	O=C–O ≈288.61 eV	C–F ≈289.87 eV	CF_2 ≈291.83 eV
GrF	0.7	1.1	–	3.2	0.8	74.6	19.6
FG/Arg-24 h	62.5	14.1	13.7	–	4.1	5.6	–
FG/Arg-48 h	58.4	15.6	17.3	–	4.4	4.3	–
FG/Arg-72 h	56.9	18.1	16.5	–	4.2	4.3	–
FG/Arg-48_K	55.9	20.1	17.2	–	4.3	2.5	–

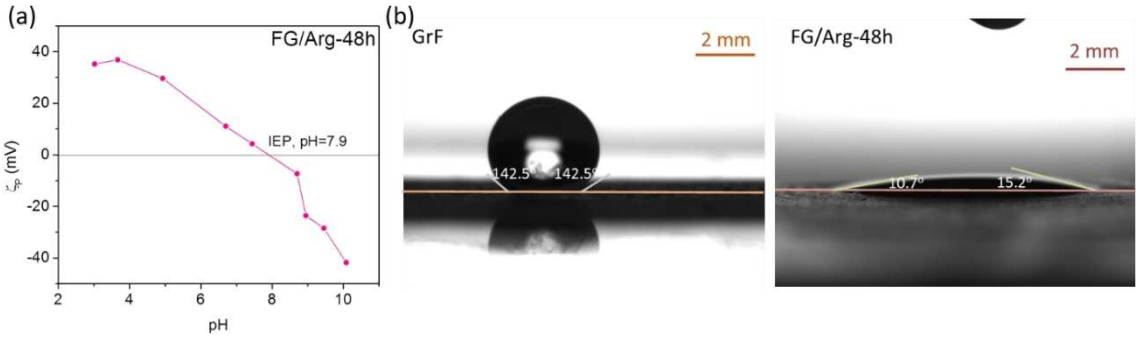

Figure 3. (a) ζp-potential curve of an FG/Arg-48 h aqueous dispersion versus pH. (b) Water droplet contact angle measurements of GrF and FG/Arg-48 h.

guanidine group. Above this pH≈8, the ζp values became negative (up to −41.8 mV).

Both FG and graphene are hydrophobic materials, whereas graphene with grafted Arg is hydrophilic and highly water dispersible. The hydrophilicity of the graphene derivatives was studied by water droplet contact angle measurements. Figure 3b shows there was a sharp change in the hydrophilicity upon Arg functionalization of the hydrophobic parent GrF, with a decrease in the water droplet contact angle from 142.5° for GF to 10.7 and 15.2° for FG/Arg-48 h. The high wettability of Arg functionalized graphene verifies the effective functionalization of hydrophobic GrF. The contact angles of all the samples prepared for different reaction times are presented in Figure S6.

The SSA of FG/Arg-48 h and FG/Arg-48 h_K was determined by N_2 adsorption/desorption measurements (Figure 4a) together with their corresponding pore size distribution (PSD) characteristics (Figure 4b). Adsorption/desorption isotherms of all the samples with PSD characteristics are shown in Figures S7 and S8, respectively. The Brunauer-Emmett-Teller (BET) surface areas of FG/Arg-24 h, FG-Arg-48 h, and FG/Arg-72 h were 61, 29, and 34 $m^2 g^{-1}$, respectively. The relatively small surface areas of the graphene derivatives may be because in the dried samples, the functionalized graphene sheets were closely associated with each other, whereas this behavior was unlikely to occur in an aqueous dispersion.[23,33] It is worth noting that the SSA decreased with increasing FD. The open isotherm of FG/Arg-48 h_K indicates slow desorption kinetics. We performed additional measurements with prolonged equilibration times (from 10 s used for all other measurements to 60 s, Figure S9). Although the equilibration time was extended considerably, the shape of isotherm remained the same. This confirms slow desorption kinetics, which may originate from the co-existence of micropores observed only in FG/Arg-48 h_K. Micropores may have been introduced by the release of CO_2 and etching from the potassium ions since the potassium carbonate is present during the material synthesis. The size of the micropores (≈ 1.5 nm) was sufficient to accommodate electrolyte ions, which is advantageous for supercapacitor electrode materials.

Scanning (SEM) and transmission electron microscopy (TEM) were employed to investigate the morphological characteristics of graphene derivatives prepared using different reaction times and with/without potassium carbonate. SEM images (Figure S10) showed the presence of platy, thin flakes of functionalized graphene with lateral sizes not exceeding 1 μm, providing evidence of satisfactory separation of the sheets. The absence of charging during the SEM imaging implied that the graphene-based sheets were electrically conductive. TEM evaluation of the FG/Arg-48 h_K sample (Figure 5a) after being

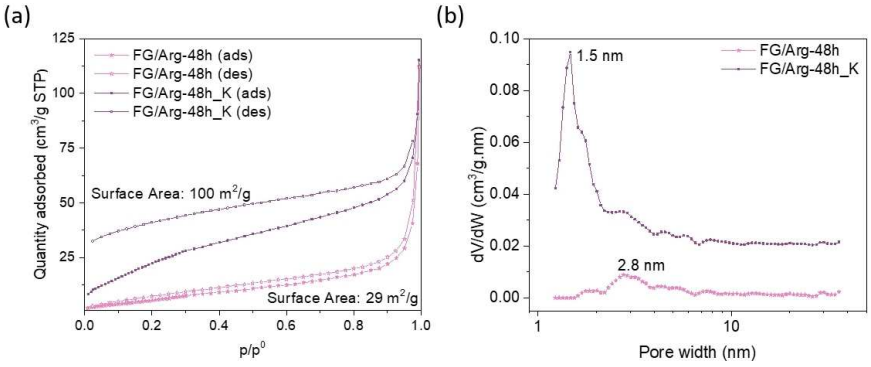

Figure 4. (a) N_2 adsorption/desorption isotherms obtained at −196 °C for FG/Arg-48 h and FG/Arg-48 h_K samples. (b) Pore size distributions of FG/Arg-48 h and FG/Arg-48 h_K samples.

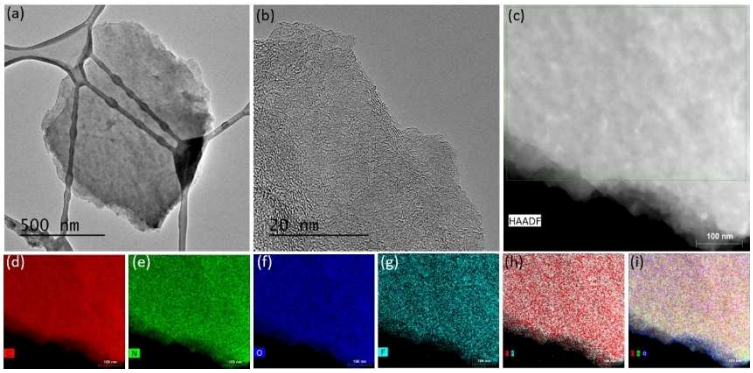

Figure 5. (a) TEM and (b) HRTEM micrographs of a FG/Arg-48 h_K sample. (c) Dark-field HRTEM image of FG/Arg-48 h_K and corresponding EDS chemical mapping: (d) carbon map, (e) nitrogen map, (f) oxygen map, (g) fluorine map, (h) carbon–fluorine map, and (i) carbon–nitrogen–oxygen overall map. (c–i) Scale bars: 100 nm.

dispersed in ethanol and then dried showed thin, almost transparent, flakes indicative of exfoliated materials. TEM images of all samples are illustrated in Figure S11. The edges of the FG/Arg-48 h_K sheets in high-resolution (HR)TEM images (Figure 5b) were almost transparent, indicative of few-layer graphene. A dark-field HRTEM image of a FG/Arg-48 h_K flake is presented in Figure 5c. The corresponding energy-dispersive X-ray spectroscopy (EDS) elemental mapping of this flake revealed homogeneous grafting of functional groups throughout the surface of the flake. Potassium was completely removed during thermal treatment with hydrochloric acid. It should be stressed the high density of functional groups were distributed uniformly across the surface without areas that were more or less densely functionalized (Figures 5d–i). This homogeneity is a major advantage of FG chemistry compared to GO chemistry.

The atomic force microscopy (AFM) image in Figure 6a,b shows a typical FG/Arg-48 h_K flake and corresponding height profile. The lateral size of the flake was around 0.8 μm and the corresponding height profile ranged from 3.9 to 11.5 nm. Assuming that the thickness of double-sided functionalized graphene with Arg was approximately 0.93 nm, the number of FG/Arg layers was estimated as ranging from 4 to 12, implying few-layer graphene. The few-layer graphene structure would be detrimental to its capacitive performance in aqueous electrolytes because it was extensively hydrated due to its high hydrophilicity attributed to Arg functionalities. A snapshot from molecular dynamics (MD) calculations (Figure 6c) illustrates the packing of double-sided functionalized FG with Arg. It was observed that arginines easily form a network of intermolecular hydrogen bonds between the layers (on average 7 H-bonds per 10 surface groups). Moreover, the material contains several intramolecular hydrogen bonds (5 intralayer H-bonds per 10 Arg groups), which may improve the final stability and structural rigidity of FG/Arg.

Figure 7a plots a set of cyclic voltammograms (CVs) recorded in 1 M H_2SO_4 (at a constant scan rate of 50 mV s^{-1}) for samples prepared with different reaction times. The potential window was fixed at 1 V to prevent the electrolysis of water. As can be seen, the CV curves featured blunt and slanted profiles with small broad redox peaks located at around 0.45 V. The deviation from the ideal rectangular shape can be explained in terms of electron spin resonance (ESR; finite resistance of the

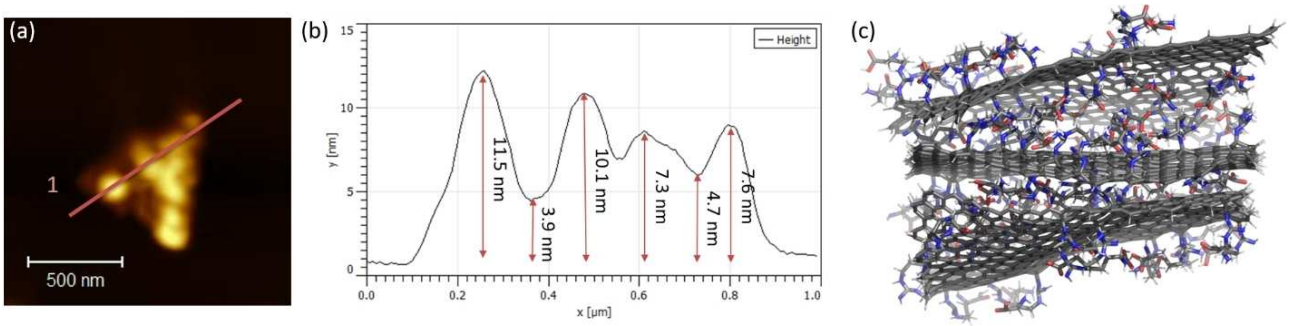

Figure 6. (a) AFM image of a representative flake and (b) corresponding height profile in direction 1. (c) Snapshot from MD simulations showing double-sided functionalized FG with Arg (solvent is not shown for clarity).

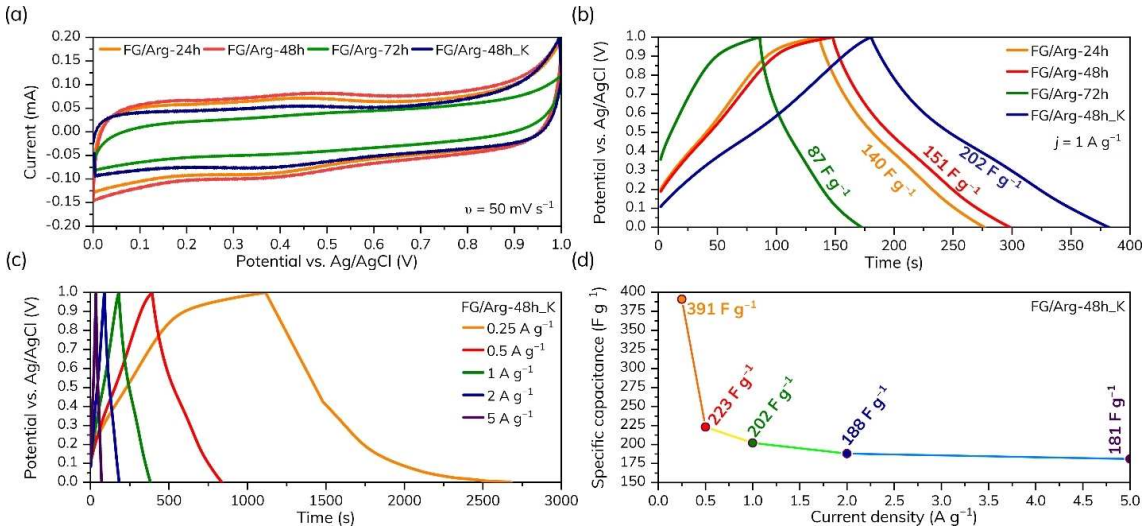

Figure 7. (a) CVs of graphene derivatives modified with Arg prepared using different reaction times. (b) GCD profiles of the prepared materials. (c) GCD profiles of FG/Arg-48 h_K recorded at current densities ranging from 0.25 to 5 A g^{-1}. (d) Corresponding specific capacitance vs. current density profile.

electrode material) and electron paramagnetic resonance (EPR; ohmic conduction across the capacitor via the electrolyte), as explained by Boonpakdee et al.,[34] while the redox response of the system reflects the presence of oxygen-containing groups[35,36] as proved by the XPS and FTIR analysis. The CV results showed that the highest current response was obtained with the sample prepared for 48 h of synthesis. Such current enhancement is connected with a higher FD because the presence of amino groups from Arg can significantly improve the electrochemical performance, especially the conductivity.[37,38] To enhance the capacitance performance of the FG/Arg-48 h sample, we prepared a sample with increased SSA and a microporous structure using potassium carbonate, as described in the previous section. As expected, such surface size enhancement decreased the FD (from 3.7 to 3.5) and affected the current response of the FG/Arg-48 h_K sample. However, a high SSA together with the high level of surface functionalization are still able to improve the capacitive performance of FG/Arg-48 h_K sample as obvious from galvanostatic charge/discharge (GCD) records (Figure 7b). Figure 7c shows GCD profiles of the "activated" sample recorded at current densities ranging from 0.25 to 5 A g^{-1}. The corresponding specific capacitance versus current density profile (Figure 7d) revealed the highest value of specific capacitance at 0.25 A g^{-1} (391 F g^{-1}). In the FG/Arg-48 h_K sample, the pore size was around 1.5 nm. Such a pore size enables sulfate ions to interact with the surface and pores of the FG/Arg-48 h_K sample, especially at a low current density, resulting in high capacitance.

Nyquist and Bode representations of impedance spectroscopy were used to provide further insights into the performance of the tested samples (Figure 8a,b). The absence of a semicircle in the high-frequency region of the Nyquist plot (Figure 8a) indicated the low resistivity of all the tested materials, in agreement with the enhanced conductivity described above. This was accompanied by a low value of ESR, particularly for the FG/Arg-48 h_K sample, as shown in Figure 8a. The slope of the impedance curve of 45° corresponded to diffusion-controlled Warburg impedance and reflected the frequency dependence of ion diffusion in the electrolyte to the electrode surface.[39,40] It is important to note that the impedance response showed a significantly shortened path for materials prepared at 24–48 h than at 72 h, indicating efficient ion transfer to the electrode surface. Further, the vertical line visible at low frequencies in the Nyquist plot indicated the capacitive behavior of the tested material. The FG/Arg-48 h_K sample showed a more vertical curve to the *y*-axis compared to the other samples, indicating that its behavior was close to that of an ideal capacitor (Figure 8a). Bode analysis in the mHz region revealed that the phase angle was −85° for the FG/Arg-48 h_K sample, as shown in Figure 8b, which is close to the value of −90° indicative of an ideal capacitor.[41] The shape of the curves in both impedance representations suggested interaction of ions at high-energy carbon sites (e.g., defects or functional groups) as well as diffusion of adsorbed electroactive species over the pore walls.[42]

A symmetric supercapacitor with 1 M H_2SO_4 as supporting electrolyte was assembled to evaluate the performance of the arginine-based graphene derivative (the cell assembly is shown in the inset of Figure 9c). Figure 9a,b shows the GCD response of FG/Arg-48 h_K in a two-electrode setup for current densities from 0.1 to 5 A g^{-1}. It can be seen that the shape of the GCD curves became more symmetrical, suggesting enhanced diffusion of the ions inside the electrochemical system. Such an observation was also reflected by the perfectly stable capacitive response across the wide range of current densities. Figure 9c shows the extraordinary life-time stability of FG/Arg-48 h_K, that is, capacitance retention of 82.3% after 30000 GCD cycles. The results from both the three- and two-electrode systems confirmed that FG modified with Arg may be an excellent candidate for supercapacitor applications.

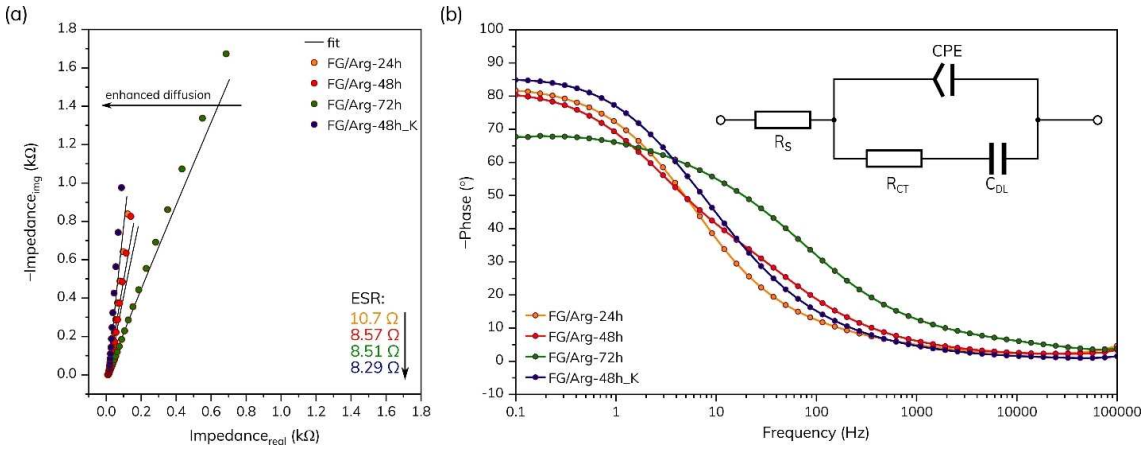

Figure 8. (a) Nyquist plots of graphene derivatives modified with Arg prepared using different reaction times. (b) Bode representation of impedance data of all the derivatives; the inset shows the electrical circuit used for data fitting.

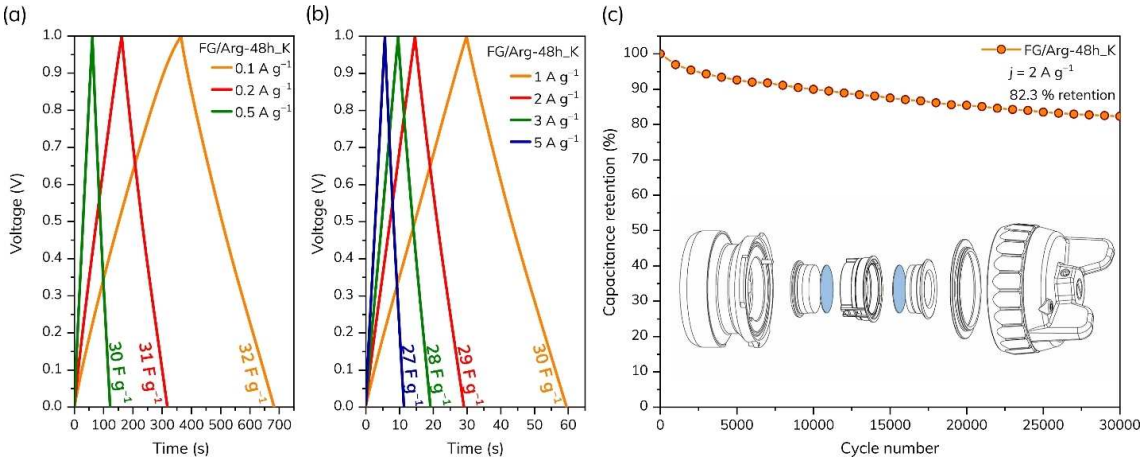

Figure 9. GCD profiles of FG/Arg-48 h_K recorded at current densities ranging from (a) 0.1–0.5 A g^{-1} and (b) 1–5 A g^{-1}. (c) Capacitance retention of FG/Arg-48 h_K after 30000 GCD cycles.

Conclusions

We report the successful covalent grafting of arginine onto a graphene surface by reaction of Boc-protected arginine with fluorographene. Arginine was grafted via its guanidine group homogeneously on both sides of graphene with around 3.7% maximum functionalization degree. This method of arginine grafting leaves both the C and N amino acid termini freely available for further chemical derivatization and introduces hydrophilic and zwitterionic groups onto a conductive graphene surface. Optimization of the composition, functionalization degree, and conductivity of the material was accomplished by monitoring the impact on capacitance performance. The best-performing sample was treated in situ with potassium carbonate, creating hierarchical micro/mesoporosity and tripling the specific surface area. This had a direct effect of boosting the capacitive performance (≈390 F g^{-1} at a current density of 0.25 A g^{-1}) because microporosity affords numerous sites for electrolyte ions adsorption, whereas mesoporosity offers ion diffusion paths and facilitates charge propagation. The principal advantage of this material was demonstrated by the durability of the assembled supercapacitor. After numerous (≈30000) charging/discharging cycles under typical operation conditions, the capacitance retention was around 82.3%. Therefore, as well as being eco-friendly, the material exhibited outstanding sustainability with promising properties for supercapacitor materials. Moreover, adopting the strategy of successful covalent grafting of small molecules on the surface of graphene lays the ground for the development of similar energy storage systems with significantly improved electrochemical performance in terms of capacitance, as well as lifetime stability of these derivatives in both aqueous and organic electrolytes.

Experimental Section

Reagents and materials

Graphite fluoride (GrF) (C/F 1:1.1), a Kaiser test kit, and Boc-Arg-OH (Boc) were purchased from Sigma-Aldrich. Acetone (pure), ethanol (absolute), *N*,*N*-dimethylformamide (DMF), and potassium carbonate were purchased from Penta. Hydrochloric acid (35%) and sulfuric acid (96%) were bought from Lachner. All reagents were used as received without further purification. All stock solutions were prepared with ultrapure water (18 MΩ cm^{-1}). The Kaiser test protocol is described in the work of Kaiser et al.[43] and recently by Soriano and Cárdenas.[44]

Synthesis of Boc- and Arg-functionalized FG

First, 200 mg of GrF was dispersed in 10 mL of DMF and subjected to ultrasonication for 10 min (Bandelin Sonoplus, type UW 3200, probe VS70T). The flask containing the dispersion was then sonicated in a sonication bath for 2.5 h (Bandelin Sonorex, DT255H type, frequency 35 kHz, power 640 W, effective power 160 W). Next, 1.76 g of Boc-Arg-OH was added to the flask and the mixture was sonicated for a further 1 h. Afterwards, the reagents were heated under stirring at 125 °C for $x = 24$, 48, or 72 h. The black product was separated by centrifugation and was purified by repeated centrifugal washings with DMF, water, and ethanol. The purified product (FG/Boc-*x*h) was transferred to a flask to which were added 20 mL hydrochloric acid (≈5.7 M) and around 3.75 mL acetone. The mixture was heated under stirring at 100 °C for 1 h to remove the Boc protecting group. Finally, the black product was isolated by centrifugation and purified by successive centrifugal washings with water, acetone, and ethanol. The purified product was labeled FG/Arg-*x*h.

Synthesis of Boc- and Arg-functionalized FG in the presence of potassium carbonate

First, 200 mg of GrF was dispersed in 10 mL of DMF and then subjected to ultrasonication for 10 min (Bandelin Sonoplus, type UW 3200, probe VS70T). The flask containing the dispersion was subsequently sonicated in a sonication bath for 2.5 h (Bandelin Sonorex, DT255H type, frequency 35 kHz, power 640 W, effective power 160 W). Next, 1.76 g of Boc-Arg-OH was added to the flask

and the mixture was sonicated for a further 1 h. Afterwards, 0.44 g of potassium carbonate in 2 mL of water was added and the mixture was sonicated for a further 15 min. Subsequently, the reagents were heated under stirring at 125 °C for 48 h. The black product was separated by centrifugation and was purified by repeated centrifugal washings with DMF, water, and ethanol. The purified product (FG/Boc-48 h_K) was then transferred to a flask to which were added 20 mL hydrochloric acid (≈5.7 M) and around 3.75 mL acetone. The mixture was heated under stirring at 100 °C for 1 h to remove the Boc protecting group. Finally, the black product was isolated by centrifugation and was purified by successive centrifugal washings with water, acetone, and ethanol. The purified product was labeled FG/Arg-48 h_K.

Characterization techniques

FTIR spectra were recorded on an iS5 FTIR spectrometer (Thermo Nicolet) using the Smart Orbit ZnSe ATR accessory. Briefly, a droplet of an ethanolic dispersion of the test material was placed on a ZnSe crystal and left to dry to form a film. Spectra were acquired by summing 100 scans obtained using N_2 gas flow through the ATR accessory. ATR and baseline correction were applied to the collected spectra.

UV/Vis absorption spectra were collected on a SPECORD S600 UV-vis spectrophotometer (Analytikjena) over the range 230–900 nm. During the Kaiser test, around 5 mg of the FG/Arg-48 h sample was placed in a test tube and then three solutions were added in the following order: (A) 75 μL of solution I (I: 10 g phenol dissolved in 20 mL ethanol), (B) 100 μL of solution II (II: 2 mL of an aqueous solution of 1 mM KCN dissolved in 98 mL of pyridine), and (C) 75 μL of solution III (III: 1.0 g of ninhydrine dissolved in 20 mL of ethanol). The test tube was incubated in a heating oil bath at 100 °C for 7 min and then removed. Next, 4.8 mL of ethanol was added to reach a final volume of 5 mL. A deep blue supernatant appeared and was separated by centrifugation and then transferred to a UV/Vis cuvette (100-QS, Suprasil, 10 mm purchased from Fischer Scientific). Finally, the UV/Vis absorption spectrum was recorded. An intense peak centered at around 583 nm was detected, verifying the presence of a primary amine group in the sample FG/Arg-48 h. For comparison, a reference Kaiser test was performed in the absence of FG/Arg-48 h, which generated a colorless solution. Further Kaiser test was performed in presence of FG/Boc-48 h (≈4 mg) where the supernatant was also colorless (Figure S1).

XPS was employed with a PHI VersaProbe II (Physical Electronics) spectrometer using an AlK_α source (15 kV, 50 W). Samples were deposited onto a silicon holder as an ethanol-based slurry, which was left to dry prior to measurement. The obtained data were evaluated and deconvoluted with the MultiPak (Ulvac - PHI, Inc.) software package. Spectral analysis included a Shirley background subtraction and peak deconvolution employing mixed Gaussian–Lorentzian functions.

Water droplet contact angle measurements were performed in a drop shape analyzer (DSA30S, Krüss, GmbH).

Raman spectra were collected using a DXR Raman spectroscope (Thermo Scientific) equipped with a laser operating at wavelength of 633 nm.

Zeta-potential (ζp) measurements were performed with a Malvern ZetaSizer Nano instrument on aqueous dispersions of around 0.03 mg mL^{-1}.

Thermal decomposition of the samples was investigated using TGA and DTG (SDT 650, TA Instruments, USA) with a sample mass of 5–10 mg. All measurements were carried out in a N_2 atmosphere with a flow rate of 100 mL min^{-1}. The heating rate was set at 5 °C min^{-1}, starting from 40 up to 1000 °C.

Surface area and pore size analyses were performed by N_2 adsorption/desorption measurements at −196 °C on a volumetric gas adsorption analyzer (3Flex, Micromeritics, USA) up to 0.965 p/p^0. Prior to the analysis, the sample was degassed under high vacuum (10^{-4} Pa) at 130 °C for 12 h, whereas high-purity (99.999%) N_2 and He gases were used for the measurements. The BET surface area was determined with respect to Rouquerol criteria[45] for the N_2 isotherm. The pore size distribution was analyzed by the N2-NLDFT 77-carbon slit pore kernel.

The samples were analyzed by SEM using a Hitachi SU6600 instrument (Hitachi, Japan) with an accelerating voltage of 5 kV. For these analyses, a drop of a dispersion of the material in ethanol was placed on a copper grid with a carbon film and dried at room temperature.

TEM images in the Supporting Information were obtained with a JEOL JEM 2100 instrument at an accelerating voltage of 200 kV. The samples were dispersed in ethanol and sonicated for 5 min. A drop of the dispersion was placed on a copper grid with a holey carbon film and dried at room temperature. STEM-HAADF (high-angle annular dark-field imaging) analyses for elemental mapping of the products was performed with a FEI Titan HRTEM microscope operated at 80 kV. Figure 5a was also obtained with FEI Titan HRTEM. For these analyses, a droplet of a dispersion of the material in ethanol with concentration of around 0.1 mg mL^{-1} was deposited onto a carbon-coated copper grid and dried.

AFM images were obtained in the amplitude-modulated semi-contact mode on an NT-MDT NTegra system equipped with a VIT–P AFM probe and using freshly cleaved muscovite mica as a substrate.

Electrochemical measurements

Three-electrode measurements were performed using a Metrohm Autolab PGSTAT128 N instrument (Metrohm Autolab B.V., Netherlands) equipped with NOVA software (version 1.11.2). Sulfuric acid with concentration $c = 1$ M was used as a supporting electrolyte. Electrochemical impedance spectroscopy (EIS) was carried out by applying an AC voltage with 5 mV amplitude and frequency range of 0.01 Hz to 100 kHz at open-circuit potential (OCP). A modified Randles circuit was used for fitting all the obtained data.

A three-electrode system was used to obtain initial information about the electrochemical behavior of the studied sample. A platinum wire electrode was used as the auxiliary electrode, whereas a Ag/AgCl electrode was used as the reference electrode. A modified glassy carbon electrode (GCE) served as the working electrode. A well homogenized dispersion of the sample in deionized water ($c \approx 2$ mg mL^{-1}) was prepared, and then 10 μL of the dispersion was drop-cast onto the surface of the GCE and left to dry at room temperature. A thin film of the sample was formed on the electrode. According to this procedure, small deviations in mass at such low concentrations and volumes can result into different masses deposited on the GCE. Furthermore, the GCE surface is fully exposed to the electrolyte and therefore possible mass losses to the electrolyte cannot be estimated. For this reason the *y*-axis in Figure 7a is not normalized as specific current (mA g^{-1}), but only current is reported. The CV curves were used in order to gain better understanding of the operation mechanism, such as the presence of the redox peaks, which are not visible in the GCD curves.

Two-electrode measurements were carried out using a BCS-810 battery tester (BioLogic Company, Seyssinet-Pariset, France) driven by BT-Lab software (version 1.65). A well homogenized dispersion (concentration 5 mg mL^{-1}) of the sample in DI water was drop-cast onto a gold electrode (diameter 18 mm) to achieve at least 1.8 mg cm^{-2} loading, then dried under an IR-lamp, followed by additional water removal in a desiccator for 2 h. Two electrodes with nearly identical loadings of the material were used to assemble a symmetrical electrochemical cell (EI-CELL GmbH, Germany) using a Whatman glass microfiber membrane (thickness 0.26 mm) as separator and 100 μL of 1 M sulfuric acid as electrolyte.

The specific capacitance C_s was calculated from GCD profiles using the following Equation (1):

$$C_s\ [\mathrm{F\ g^{-1}}] = \frac{I \times \Delta t}{m \times \Delta V} \quad (1)$$

where I is the applied current [A], Δt is the discharge time [s], m is the mass of total electrode material [g] (on both electrodes in a two-electrode system), and ΔV is the potential window [V].

Theoretical calculations

MD simulations were carried out in Gromacs 5.0 software[46] using the Amber99 force field.[47] Aromatic carbons in the graphene layer were modeled as uncharged LJ spheres using the modified Cheng and Steele parameters for graphitic carbons.[48] The dimensions of graphene were assumed to be approximately 4×4 nm with a functionalization degree of 3.5%. In the initial geometry, three sheets of FG/Arg were placed in the middle of a square box (a = 7.5 nm) and solvated with TIP4P water.[49] Periodic boundary conditions were applied in all directions. First, the system was minimized and thermalized at 300 K under the NpT ensemble. This was followed by a 30 ns production run under the NVT ensemble. The Lennard–Jones (LJ) potential was used for atomic interactions. Long-range electrostatic interactions were treated by the particle-mesh Ewald (PME) technique. Cut-off distances for LJ interactions and the real space term of the PME were set to 1 nm. Temperature and pressure were maintained using the V-rescale thermostat[50] and Berendsen barostat with isotropic scaling (1 bar),[51] respectively. Hydrogen atoms were constrained by the LINCS algorithm.[52] The Newtonian equations of motion were integrated with a 2 fs time step.

Acknowledgements

We acknowledge financial support from the ERDF/ESF project "Nano4Future" of the Ministry of Education, Youth, and Sports of the Czech Republic (CZ.02.1.01/0.0/0.0/16_019/0000754) and an ERC project (683024) as part of the H2020 program. V.Š. thanks the Internal Student Grant Agency of Palacký University in Olomouc, Czech Republic (IGA_PrF_2021_031). R.Z. and A.B. acknowledge funding from the Czech Science Foundation, project GA CR – EXPRO, 19-27454X. The authors also acknowledge partial support provided by the Research Infrastructure NanoEnviCz project funded by the Ministry of Education, Youth and Sports of the Czech Republic (No. LM2018124). We thank Mgr. Jana Stráská, Dr. Eirini Ioannou, Dr. Martin Petr, and Dr. Zuzana Chaloupková for TEM, SEM, XPS, and Raman measurements.

Conflict of Interest

The authors declare no conflict of interest.

Keywords: arginine · fluorographene · graphene · supercapacitor · ultracapacitor

[1] G. Luderer, M. Pehl, A. Arvesen, T. Gibon, B. L. Bodirsky, H. S. de Boer, O. Fricko, M. Hejazi, F. Humpenöder, G. Iyer, S. Mima, I. Mouratiadou, R. C. Pietzcker, A. Popp, M. van den Berg, D. van Vuuren, E. G. Hertwich, *Nat. Commun.* **2019**, *10*, 5229.
[2] Y. Luo, C. Yang, Y. Tian, Y. Tang, X. Yin, W. Que, *J. Power Sources* **2020**, *450*, 227694.
[3] M. Sethi, U. S. Shenoy, D. K. Bhat, *J. Alloys Compd.* **2021**, *854*, 157190.
[4] J. Acharya, T. H. Ko, M.-K. Seo, M.-S. Khil, H.-Y. Kim, B.-S. Kim, *ACS Appl. Mater. Interfaces* **2020**, *3*, 7383.
[5] J. Han, Y. Ping, S. Yang, Y. Zhang, L. Qian, J. Li, L. Liu, B. Xiong, P. Fang, C. He, *Diamond Relat. Mater.* **2020**, *109*, 108044.
[6] N. Kamboj, T. Purkait, M. Das, S. Sarkar, K. S. Hazra, R. S. Dey, *Energy Environ. Sci.* **2019**, *12*, 2507.
[7] C. Liu, Z. Yu, D. Neff, A. Zhamu, B. Z. Jang, *Nano Lett.* **2010**, *10*, 4863.
[8] A. K. Geim, K. S. Novoselov, *Nat. Mater.* **2007**, *6*, 183.
[9] J.-U. Lee, D. Yoon, H. Cheong, *Nano Lett.* **2012**, *12*, 4444.
[10] A. Emadi, B. Honarvar, M. Emadi, M. Nafar, *Russ. J. Appl. Chem.* **2020**, *93*, 1160.
[11] L. Hou, C. Kong, Z. Hu, Y. Yang, H. Wu, Z. Li, X. Wang, P. Yan, X. Feng, *Appl. Surf. Sci.* **2020**, *508*, 145192.
[12] D. M. El-Gendy, N. A. A. Ghany, E. E. F. El Sherbini, N. K. Allam, *Sci. Rep.* **2017**, *7*, 43104.
[13] L. Deng, C. Zhou, Z. Ma, G. Fan, *J. Colloid Interface Sci.* **2020**, *561*, 416.
[14] X. Zhou, T. Meng, F. Yi, D. Shu, D. Han, Z. Zhu, A. Gao, C. Liu, X. Li, K. Yang, H. Yi, *J. Power Sources* **2020**, *475*, 228554.
[15] Q. Wang, H. Gao, C. Zhao, H. Yue, G. Gao, J. Yu, Y.-U. Kwon, Y. Zhao, *Electrochim. Acta* **2021**, *369*, 137700.
[16] Y. Yang, W. Ma, H. Zhu, H. Meng, C. Wang, F. Ma, Z. Hu, *New J. Chem.* **2020**, *44*, 16821.
[17] A. B. Bourlinos, A. Bakandritsos, N. Liaros, S. Couris, K. Safarova, M. Otyepka, R. Zbořil, *Chem. Phys. Lett.* **2012**, *543*, 101.
[18] A. B. Bourlinos, K. Safarova, K. Siskova, R. Zbořil, *Carbon* **2012**, *50*, 1425.
[19] K. E. Whitener, R. Stine, J. T. Robinson, P. E. Sheehan, *J. Phys. Chem. C* **2015**, *119*, 10507.
[20] M. Medveď, G. Zoppellaro, J. Ugolotti, D. Matochová, P. Lazar, T. Pospíšil, A. Bakandritsos, J. Tuček, R. Zbořil, M. Otyepka, *Nanoscale* **2018**, *10*, 4696.
[21] D. Matochová, M. Medved', A. Bakandritsos, T. Steklý, R. Zbořil, M. Otyepka, *J. Phys. Chem. Lett.* **2018**, *9*, 3580.
[22] A. Bakandritsos, D. D. Chronopoulos, P. Jakubec, M. Pykal, K. Čépe, T. Steriotis, S. Kalytchuk, M. Petr, R. Zbořil, M. Otyepka, *Adv. Funct. Mater.* **2018**, *28*, 1801111.
[23] E. C. Vermisoglou, P. Jakubec, A. Bakandritsos, M. Pykal, S. Talande, V. Kupka, R. Zbořil, M. Otyepka, *Chem. Mater.* **2019**, *31*, 4698.
[24] K. Hou, P. Gong, J. Wang, Z. Yang, Z. Wang, S. Yang, *RSC Adv.* **2014**, *4*, 56543.
[25] A. R. Rafieerad, A. R. Bushroa, A. Amiri, K. Kalaiselvam, K. Vellasamy, J. Vadivelu, *J. Hazard. Mater.* **2018**, *360*, 132.
[26] D. Chen, Q. Chen, T. Liu, J. Kang, R. Xu, Y. Cao, M. Xiang, *RSC Adv.* **2019**, *9*, 20149.
[27] C. J. Pandian, R. Palanivel, *J. Exp. Nanosci.* **2016**, *11*, 1193.
[28] K. Manzoor, M. Ahmad, S. Ahmad, S. Ikram, *RSC Adv.* **2019**, *9*, 7890.
[29] X. Li, G. Jiang, X. Shen, G. Li, *ACS Sustainable Chem. Eng.* **2020**, *8*, 1899.
[30] T. Nakajima, V. Gupta, Y. Ohzawa, H. Groult, Z. Mazej, B. Žemva, *J. Power Sources* **2004**, *137*, 80.
[31] J. Zhu, H. Zhang, R. Chen, Q. Liu, J. Liu, J. Yu, R. Li, M. Zhang, J. Wang, *J. Colloid Interface Sci.* **2019**, *543*, 192.
[32] M. Zhang, Y. Ma, Y. Zhu, J. Che, Y. Xiao, *Carbon* **2013**, *63*, 149.
[33] A. Bakandritsos, M. Pykal, P. Błoński, P. Jakubec, D. D. Chronopoulos, K. Poláková, V. Georgakilas, K. Čépe, O. Tomanec, V. Ranc, A. B. Bourlinos, R. Zbořil, M. Otyepka, *ACS Nano* **2017**, *11*, 2982.
[34] D. Boonpakdee, C. F. Guajardo Yévenes, W. Surareungchai, C. La-o-vorakiat, *J. Mater. Chem. A* **2018**, *6*, 7162.

[35] Y. J. Oh, J. J. Yoo, Y. I. Kim, J. K. Yoon, H. N. Yoon, J.-H. Kim, S. B. Park, *Electrochim. Acta* **2014**, *116*, 118.
[36] Y.-H. Lee, K.-H. Chang, C.-C. Hu, *J. Power Sources* **2013**, *227*, 300.
[37] M. Yu, Z. Wang, H. Zhang, P. Zhang, T. Zhang, X. Lu, X. Feng, *Nano Energy* **2019**, *65*, 103987.
[38] M. Yang, Z. Zhou, *Adv. Sci.* **2017**, 10.
[39] L. Zhang, G. Shi, *J. Phys. Chem. C* **2011**, *115*, 17206.
[40] Y. Wang, Z. Shi, Y. Huang, Y. Ma, C. Wang, M. Chen, Y. Chen, *J. Phys. Chem. C* **2009**, *113*, 13103.
[41] J. Zhang, X. S. Zhao, *ChemSusChem* **2012**, *5*, 818.
[42] A. Eftekhari, *ACS Sustainable Chem. Eng.* **2019**, *7*, 3692.
[43] E. Kaiser, R. L. Colescott, C. D. Bossinger, P. I. Cook, *Anal. Biochem.* **1970**, *34*, 595.
[44] M. L. Soriano, S. Cárdenas, *J. Carbon Res.* **2019**, *5*, 68.
[45] J. Rouquerol, F. Rouquerol, P. Llewellyn, G. Maurin, K. S. W. Sing, *Adsorption by Powders and Porous Solids: Principles, Methodology and Applications*, Elsevier Science, **2013**.
[46] D. Van Der Spoel, E. Lindahl, B. Hess, G. Groenhof, A. E. Mark, H. J. C. Berendsen, *J. Comput. Chem.* **2005**, *26*, 1701.
[47] W. D. Cornell, P. Cieplak, C. I. Bayly, I. R. Gould, K. M. Merz, D. M. Ferguson, D. C. Spellmeyer, T. Fox, J. W. Caldwell, P. A. Kollman, *J. Am. Chem. Soc.* **1995**, *117*, 5179.
[48] A. Cheng, W. A. Steele, *J. Chem. Phys.* **1990**, *92*, 3858.
[49] W. L. Jorgensen, J. Chandrasekhar, J. D. Madura, R. W. Impey, M. L. Klein, *J. Chem. Phys.* **1983**, *79*, 926.
[50] G. Bussi, D. Donadio, M. Parrinello, *J. Chem. Phys.* **2007**, *126*, 014101.
[51] H. J. C. Berendsen, J. P. M. Postma, W. F. van Gunsteren, A. DiNola, J. R. Haak, *J. Chem. Phys.* **1984**, *81*, 3684.
[52] B. Hess, H. Bekker, H. J. C. Berendsen, *J. Comput. Chem.* **1997**, *18*, 1463.

Manuscript received: May 18, 2021
Revised manuscript received: June 18, 2021
Accepted manuscript online: July 20, 2021
Version of record online: August 18, 2021